

Self-Powered Colloidal Wurtzite-Structure Quantum Dots Photodetectors Based On Photoinduced-Pyroelectric Effect

Lufan Jin, Yating Zhang,* Yu Yu, Zhiliang Chen, Yifan Li, Mingxuan Cao, Yongli Che, and Jianquan Yao

Colloidal wurtzite-structure CdSe/ZnS quantum dots (CWQDs), with noncentral asymmetry structure and spontaneous polarization, have an extensive potential for applications based on the pyroelectric effect, such as energy harvesters, self-powered nanogenerators, and photosensors. Here, a low-cost, easy-fabrication, and high-speed self-powered photodetector is demonstrated, which performs independently without any external power source. The response of the device caused by the photoinduced-pyroelectric effect is experimentally investigated based on the Au/CWQDs/Au edge-electrodes structure, which exhibits an ultrafast photoresponse with a rising time of 20.6 μs and a falling time of 30.1 μs . Moreover, the frequency and temperature dependence of the device also is investigated under zero bias. This work provides a new approach to achieve self-powered photodetectors, which may show promise for extensive batch applications, such as wireless sensing, optothermal detection, optoelectronic communication, and energy harvesting.


The pyroelectric detectors have been researched for several decades due to the ability of converting the thermal fluctuation, caused by ambient energy such as solar and thermal, into free charge carriers.^[1] Now, due to the infinite demand of energy harvesters, detectors, and sensors, extensive attentions have been directed to develop new low-cost, easy-fabrication, and high-speed pyroelectric detectors with various novel nanomaterials such as quantum dots (QDs),^[2-4] nanowires (NW),^[5,6] nanorods (NR),^[7,8] and so on. Among these nanomaterials, quantum dots, known as quasi-zero-dimension material, exhibit tunable bandgap, high thermal and optoelectronic efficiency, and short charge carrier lifetime owing to quantum confinement. Colloidal wurtzite-structure quantum dots (CWQDs), with noncentral asymmetry structure and spontaneous polarization, like CdS, CdSe, ZnS, and ZnO, have

the potential to scavenge energy by utilizing pyroelectric effect.^[9,10] Compared with polar materials including lead zirconate titanate, barium strontium titanate, barium titanate,^[11-15] the photodetectors with colloidal wurtzite-structure CdSe/ZnS quantum dots have its advantages, including low cost, easy manufacture, and wide applied fields. Due to the quantum confinement property, size dependence of QDs decides the optoelectronic properties means that CdSe/ZnS QDs can be artificially manufactured by their sizes, shapes, and capping ligands to meet the sundry occasions.^[16] Identically, CWQDs have the potential ability to convert thermal fluctuation into electric energy (measurable electric signal) by the pyroelectric effect, which is triggered from the temperature fluctuation (dT/dt), not the overall temperature variation (ΔT).^[17,18] Moreover, self-powered property of photodetectors (PDs) based on CWQDs can be realized through thermal fluctuation of materials induced from light. CWQDs with tunable bandgap could extend the response spectra to longer wavelengths from UV to near infrared ray. However, up to now, there is few report about pyroelectric photodetector based on CWQDs.^[19] Therefore, it provides an unprecedented and effective alternative to achieve newly pyroelectric photodetector through exploring the photoinduced-pyroelectric effect of CWQDs.

For most optical materials, the absorption of the incident photon can result in temperature variation (ΔT). Furthermore, due to accompanying time varying of internal electric field, pyroelectric polarization within nonsymmetric structure materials can be induced by time-dependent temperature fluctuation (dT/dt).^[20,21] The bound charges by spontaneous polarization will be vanished by equivalent floating electric charges from the interface on the thermal equilibrium condition, presented as no electricity macroscopically. Moreover, the self-powered Au/CWQDs/Au PDs devices under a modulated incident 532 nm light obviously have the ability to give rise to time-dependent temperature fluctuation (dT/dt), which will accordingly change the intensity of spontaneous polarization, leading to the floating free electric charges incompletely shielding bound charges.^[22,23] The intensity change of pyroelectric polarization can modulate the photon-generated charge transmission. Then, the internal electric field emerges because of the additional free charges attracting or repelling the charge particle in the adjacent space. When the device is connected to an external circuit, the free

L. Jin, Dr. Y. Zhang, Y. Yu, Z. Chen, Y. Li, M. Cao, Y. Che, Prof. J. Yao
Institute of Laser and Opto-Electronics
School of Precision Instruments and Opto-electronics Engineering
Tianjin University
Tianjin 300072, China
E-mail: yating@tju.edu.cn

L. Jin
Department of Material Engineering
Zhejiang Industry and Trade Vocational College
Wenzhou 325003, China

 The ORCID identification number(s) for the author(s) of this article can be found under <https://doi.org/10.1002/adom.201800639>.

DOI: 10.1002/adom.201800639

charges on its Au electrodes will be redistributed to compensate for the change in bound charges, leading to a pyroelectric current flow in the circuit, and therefore the short-circuit current output can be obtained.^[24]

In this work, colloidal wurtzite-structure CdSe/ZnS quantum dots and MEH-PPV (Poly[2-methoxy-5-(2-ethylhexyloxy)-1,4-phenylenevinylene]) are combined to fabricate a self-powered 532 nm light photodetector. There is a pair of novel pyroelectric currents (negative current is 28.3 nA and positive current is 23 nA) under the light intensity of 322.5 mW cm⁻². The pyroelectric effect is systematically researched by turning-on or -off modulation of 532 nm light illumination to achieve self-powered PDs. The schematic diagram of the experimental device of investigating the Au/CWQDs/Au self-powered photodetectors based on photoinduced pyroelectric effect is displayed in Figure S1 (Supporting Information). The minimum photoresponse time of the self-powered Au/CWQDs/Au PDs is respectively measured to be 20.6 μs for a rising time and 30.1 μs for a falling time, respectively. Furthermore, the photoresponse of the self-powered Au/CWQDs/Au PDs is studied under different frequency of light illumination and temperature of device. When the temperature increases from 22 to 34 °C, the negative current and positive current are increased by 19% and 21%, respectively. The modulation frequency dependence of the light illumination also is researched experimentally from 100 Hz to 3 kHz. This work reveals a potential possibility to apply CWQDs to a self-powered PD, clarifying profoundly the photoinduced pyroelectric effect of the self-powered Au/CWQDs/Au PDs and exploring the photoresponse of PDs with different frequency and temperature.

Figure 1a illustrates the structure of the layered side-structure self-powered nanogenerator with illustrations of device photograph. First, Au electrodes array is fabricated by the thermal evaporation method on the silica layer with good insulation and Si substrate. Then, the Colloidal wurtzite-structure CdSe/ZnS quantum dots and MEH-PPV (poly[2-methoxy-5-(2-ethylhexyloxy)-1,4-phenylenevinylene]) are synthesized via a hydrothermal method by the spin-coating process at 5 min intervals to form the Au/CWQDs/Au Schottky junction. The detailed fabrication process can be discovered in the Experimental Section. The average thickness of the quantum dot layer in Figure 1b is 19 nm measured via atomic force microscope (AFM). The transmission electron microscope (TEM) image presented in Figure 1c indicates the sizes of QDs are approximately equal to 5 nm, which shows the QDs are produced with a small size distribution and are not agglomerated for the TOPO (triethylphosphine oxide) dispersant. The identity distance of CdSe/ZnS core/shell QDs is calculated to be 0.229 nm, corresponding to the crystal face (111) of wurtzite structure. The X-ray diffraction (XRD) with three peaks at 26.42°, 43.72°, and 51.41° is demonstrated in Figure S2 (Supporting Information), which correspond to (111), (220), and (311) of cubic wurtzite structure, respectively. According to the Scherrer equation, the average diameter of the QDs is calculated to be 5.3 nm, which also matches the observed result from the TEM image. The energy band diagram of layered hybrid is shown in Figure 1d, which shows that the HOMO/LUMO values of QDs are -3.5 and -5.7 eV.^[25] Since the conduction band of QDs is below MEH-PPV, the photogenerated electron is easily

transferred to QDs surface from MEH-PPV. Therefore the existence of MEH-PPV provides more charges to take part in the pyroelectric process. The optical absorption spectrum of QDs/MEH-PPV layered films is shown in Figure 1e. For the sake of comparison, the absorption spectrum of pure QDs film has also shown in the figure. It is observed that the overall absorption of the film with MEH-PPV increases, but no shift in absorption peak at 550 nm. *I*-*V* characteristics of the self-powered Au/CWQDs/Au PD under dark and several different power densities of 532 nm light illumination are measured and the results are shown in Figure 1f. As can be clearly seen, the PD has a superior photoresponse property. Interestingly, the photoresponse current of the PD device is slightly higher under the negative voltage bias than that under the positive voltage bias, shown in the illustration, which indicates that the photogenerated electron is more easily to be transferred.

The pyroelectric performance of the self-powered Au/CWQDs/Au PD device has been demonstrated under bias-free condition. Several periods of output current response of the PD under the illumination of 322.5 mW cm⁻² are scrupulously investigated and plotted in **Figure 2a** by periodically shielded and unshielded the 532 nm light via an optical chopper at the frequency of 2 kHz. One typical period of the short-circuit *I*-*t* curve intercepted from Figure 2a is plotted in Figure 2b, which intuitively exhibits that a zooming current peak is generated when the 532 nm light is turned on, reaching to a magnitude of $I_{py+} = 23$ nA. This is due to the fact that when the light strikes on the PD with a rapid rise in temperature, the time-dependent temperature fluctuation is emerging and increasing with the increasing light receiving area. Then, a pyroelectric electric field within the CWQDs layer would be achieved, which can effectively drive the flow of electrons through external circuits and generate the pyroelectric current. The pyroelectric current can be expressed as $I_{py} = S\gamma(dT/dt)$, where *S* is the effective receiving area and γ is the pyroelectric coefficient. So, the pyroelectric current I_{py} is proportional to the time-dependent temperature fluctuation *dT/dt*. After that, due to the light absorption saturation, *dT/dt* gradually decreases to zero, so do the current. So, when the chopper frequency is low enough, the above process can be found, as shown in the inset of Figure 2b. Whereafter, while the 532 nm light is suddenly turned off, an inverse current is induced because of the negative time-dependent temperature fluctuation (*dT/dt* < 0) caused by the inverse electric field and reaches to an inverse maximum ($I_{py-} = -28.3$ nA). At last, the pyroelectric current is gradually decreasing to zero until the light restart illuminating the PD. This overall process will periodically repeat. So in order to validate that the current is only caused by the pyroelectric effect and not by other effects, the response of the self-powered Au/CWQDs/Au PD device is studied under three different conditions: dark, continuous light illumination, and light illumination with the chopper chopping, as shown in Figure S3 (Supporting Information). The long-term stability and repeatability of the self-powered Au/CWQDs/Au PD device is demonstrated by measuring dozens of cycles of the short-circuit *I*-*t* under the light chopping frequency of 100 Hz, as shown in Figure S4 (Supporting Information). Furthermore, the response time of the device is also shown in Figure 2b, including the rising time and the falling time, which manifests the transient response characteristic of the pyroelectric

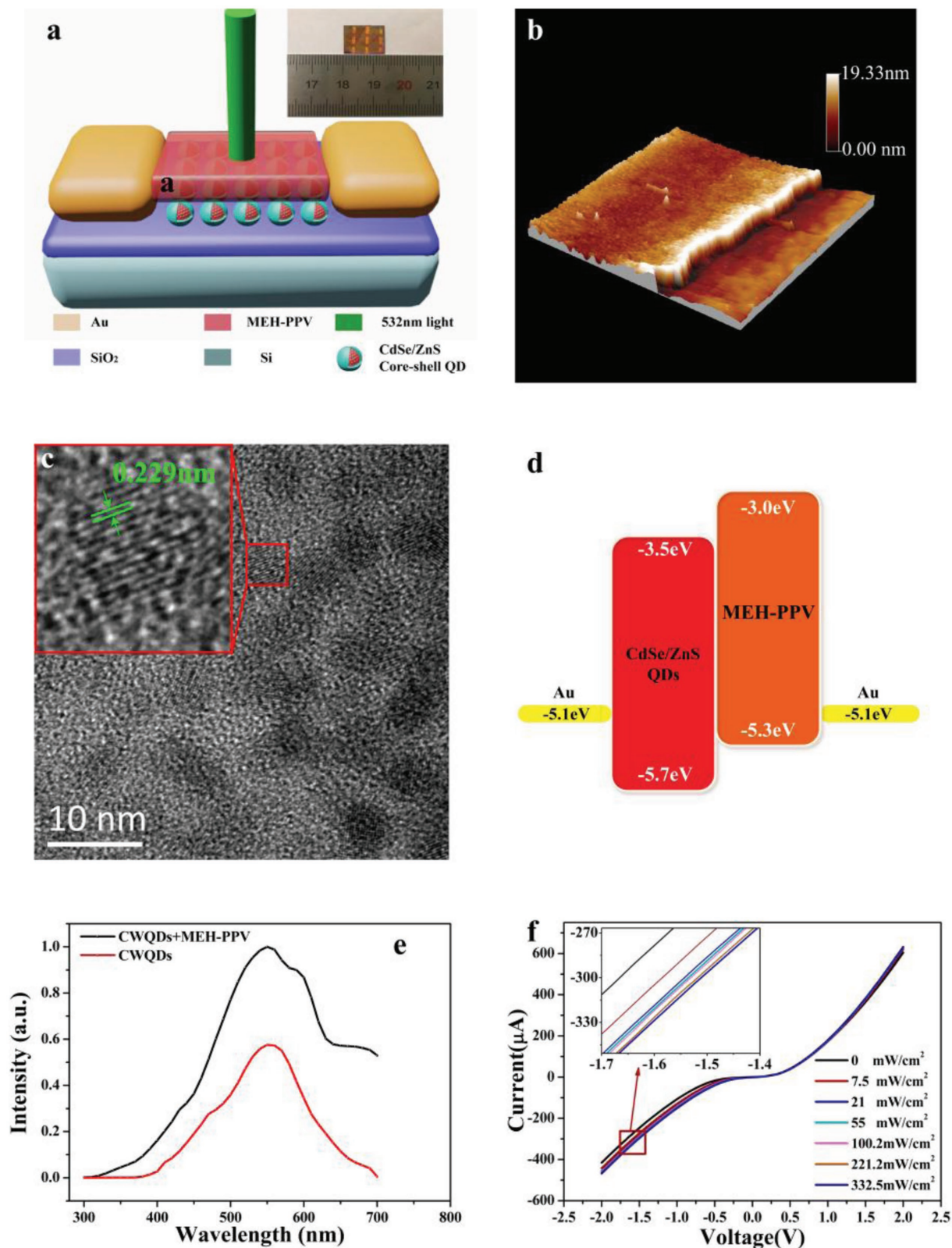


Figure 1. Schematic, digital images, and photoresponse characteristics of the self-powered Au/CWQDs/Au photodetectors. a) Schematic and digital images of the self-powered Au/CWQDs/Au PD devices. b,c) AFM and TEM images of CWQDs layer. d) Energy band diagram of the Au/CWQDs/Au PD. e) The absorption spectrum of CWQDs and CWQDs+MEH-PPV. f) Typical I - V characteristics of the PD under dark and a series of 532 nm light intensities

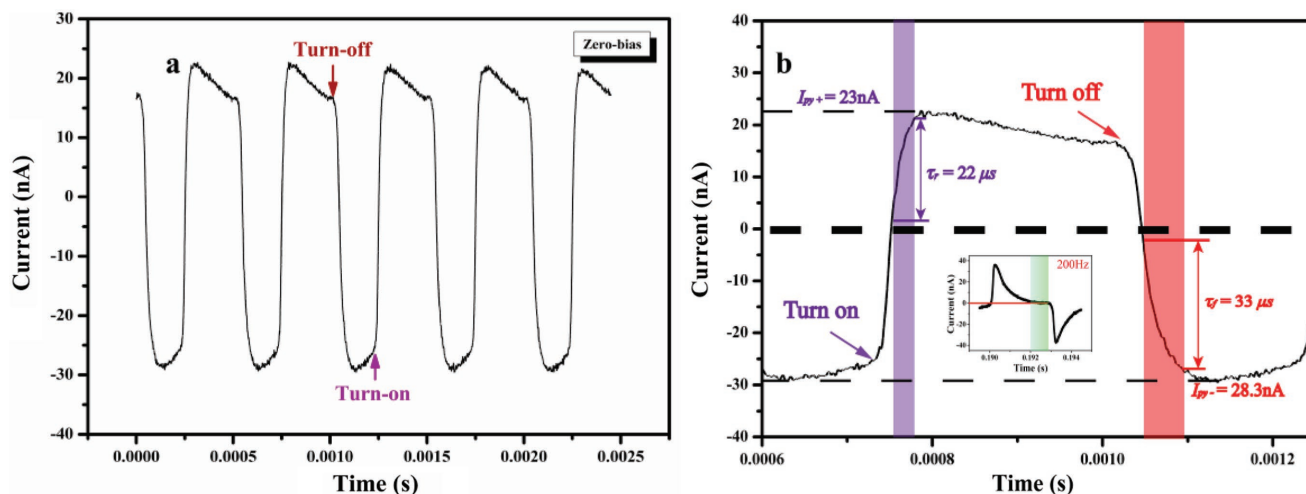


Figure 2. a) Under bias-free conditions, the output-current response of the self-powered PDs under periodical 532 nm illumination of 322.5 mW cm^{-2} . b) One typical cycle of the short-circuit $I-t$ curve.

detector for the time-dependent temperature fluctuation. So in general, the rising time is defined as 10% to 90% of the time duration from the moment of turning on the light to the moment of reaching its positive maximum of the pyroelectric current. The time is measured to be about $22 \mu\text{s}$ under 2 kHz light chopping frequency. Analogously, the falling time is about $33 \mu\text{s}$, which is defined as the 10% to 90% of the time duration from the moment of turning off to the moment of reaching its negative maximum.^[26,27] According to previous studies,^[28] the response speed of the pyroelectric device is restricted by the interelectrode capacitance. So, this ultrafast response speed of the Au/CWQDs/Au pyroelectric PD is attributed to the edge-electrode structure with low capacitance.

Figure 3 illustrates an operation cycle of pyroelectric effect for the self-powered Au/CWQDs/Au PDs with schematically illustrations of current and the charge distribution in each state. First, the process 1 indicates that when the chopper blade gradually is not shielding light illumination, the receiving area of CWQDs layer is increasing, resulting in the increasing temperature. As the time-dependent temperature fluctuation (dT/dt) is increasing, the electric dipole will extremely oscillate on the respective axis of symmetry in some degree. Then the induced charge will decrease at the electrode for the depressed overall average polarization intensity to form the built-in electric field.^[29] Consequently, the pyroelectric current is rapidly increasing as the time-dependent temperature fluctuation (dT/dt) quickly rises. Then, when the chopper blade is no longer shielding the light, the time-dependent temperature fluctuation (dT/dt) reaches its maximum, so do the current, shown in the segment A of the illustration. Afterward, although the light of the upright incidence illuminates on the material completely, the current is decreasing slowly because of the decreasing time-dependent temperature fluctuation (dT/dt), shown as the segment B, which is caused by the saturation of the photons absorption as shown in the process 2. Next, the process 3 shows that when the chopper blade begins to shielding the light, the decreasing temperature fluctuation makes the oscillation amplitude of electric dipole becoming less, and then the sign of pyroelectric current is reversed to its maximum,

shown as the segment C.^[30] Finally, the blade shields the light completely, leading to temperature of the device slowly decreasing as shown the process 4. So, the current shows as the segment D is decreasing till the light illumination again on CWQDs PDs. The process line of 1-2-3-4 covers one typical cycle of the pyroelectric effect of the self-powered Au/CWQDs/Au PDs including the current and the charge distribution.^[31]

To demonstrate the pyroelectric performance of the Au/CWQDs/Au photodetectors, the relationship between the pyroelectric current and incident light intensity is probed and the plot of the short-circuit current response with different 532 nm light illumination intensity from 7.5 to 332.5 mW cm^{-2} is shown in **Figure 4a**. It shows that the Au/CWQDs/Au photodetector reveals an outstanding distinguishable response under various light intensities. The whole current of one cycle increases with the increasing light intensity, which appears to be a positive linear relationship after an accurate calculation, as depicted in **Figure 4b** (navy line). The device shows the maximum negative current and positive current are $\approx 28.7 \text{ nA}$ ($I_{\text{py-}}$) and $\approx 21.5 \text{ nA}$ ($I_{\text{py+}}$) at the maximum light intensity of 332.5 mW cm^{-2} . In addition, the photoresponse performances of the photodetector including the photoconductive gain G , the photoresponsivity R , specific detectivity D^* , given as $G = (I_{\text{py}}/e)/(ES/h\nu)$, $R = I_{\text{py}}/(ES)$, and $D^* = R/(2e \cdot I_{\text{dark}}/S)$,^{0.5} respectively, are precisely calculated from **Figure 4a**, where I_{py} is the pyroelectric current defined as the $|I_{\text{light}} - I_{\text{dark}}|$, e is the elementary charge, E is the incident light intensity, h is the Planck constant, ν is the photon frequency, S is the effective area of the detector ($2 \text{ mm} \times 2 \text{ mm}$), I_{dark} is the dark current in the order of 10^{-11} A .^[32-34] **Figure 4b,c** separately present the G , R , and D^* of the positive current $I_{\text{py+}}$ and negative current $I_{\text{py-}}$ at different 532 nm light intensities, labeled as $G_{\text{py+}}$ and $G_{\text{py-}}$, $R_{\text{py+}}$ and $R_{\text{py-}}$, and $D^*_{\text{py+}}$ and $D^*_{\text{py-}}$, respectively. The photoconductive gain G measured through experiments is approximately an inverse proportion to the incident light intensity, matching to the fitting curve (red line in **Figure 4b**). As shown, the photoconductive gain G tends to be saturated with increasing the incident light intensity, to be 5.04×10^{-6} ($G_{\text{py-}}$) and 3.59×10^{-6} ($G_{\text{py+}}$). Both of R and D^* exhibit decreasing tendency with the increasing

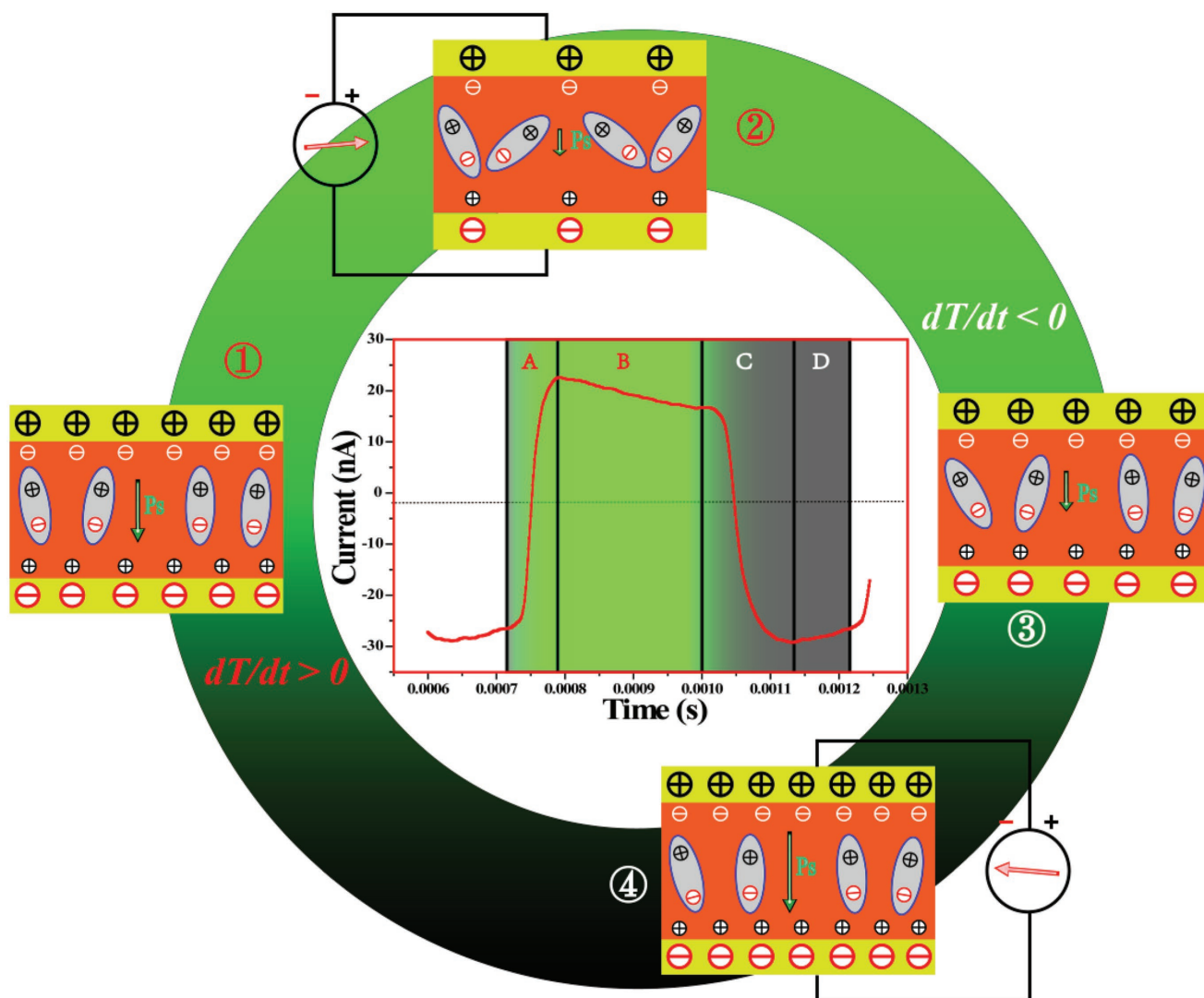


Figure 3. A typical operation cycle of pyroelectric effect for Au/CWQDs/Au photodetectors with schematical illustrations of current and the charge distribution in each state.

light intensity due to photogenerated charge saturation, to its steady value ($R_{py+} = 1.55 \times 10^{-6}$ A/W and $R_{py-} = 2.17 \times 10^{-6}$ A W⁻¹ and $D^*_{py+} = 1.73 \times 10^6$ Jones, and $D^*_{py-} = 2.43 \times 10^6$ Jones, respectively) under illumination of 332.5 mW cm⁻². The response time of the pyroelectric photodetector is expressed as the response speed of the detector for the time-dependent temperature fluctuation, which is the relaxation time of the output signal of the detector illuminated by a sudden radiation. The response time of the Au/CWQDs/Au photodetector under a series of different modulation frequency from 100 Hz to 3 kHz, including the rising time and falling time, is systematically investigated and plotted in Figure 4d. Interestingly, the response time is approximately inversely proportion to the modulation frequency, the fitting curves displayed in the figure (red line), which signify that the response time decreases with the increase of modulation frequency and can be extremely tiny. However, in this work, limited by the chopper frequency (3 kHz), the minimum of response time is to be 20.6 μ s for the rising time and 30.1 μ s for the falling time.

It has been theoretically deduced that the relationship between the responsivity of the pyroelectric detector and the modulation frequency is approximately inverse ratio at high frequency band: $R_1 \approx \alpha\gamma S/\omega HC$,^[35] where α is the absorptivity, ω is the modulation frequency, H is the thermal capacity, and C is the effective capacitance. So, a typical cycle of the short-circuit $I-t$ curve of the self-powered Au/CWQDs/Au PDs under a series of different modulation frequency is demonstrated and displayed in Figure S5 (Supporting Information). It shows that the current decreases as the frequency increases. The relationship of the responsivity $R(\omega)$ with the frequency is obtained from Figure S5 and plotted in Figure 5a. Obviously, the current responsivity decrease with the increasing modulation frequency, labeled as $R(\omega)_{py+}$ and $R(\omega)_{py-}$ expressing the positive and the negative. $R(\omega)_{py-}$ is always a little bigger than $R(\omega)_{py+}$, and the gap between them is less at the frequency band from 100 Hz to 1 kHz, which is widening as the frequency increases. After being calculated, the responsivity $R(\omega)_{py-}$ reaches its maximum at 100 Hz, as well as the responsivity $R(\omega)_{py+}$ to

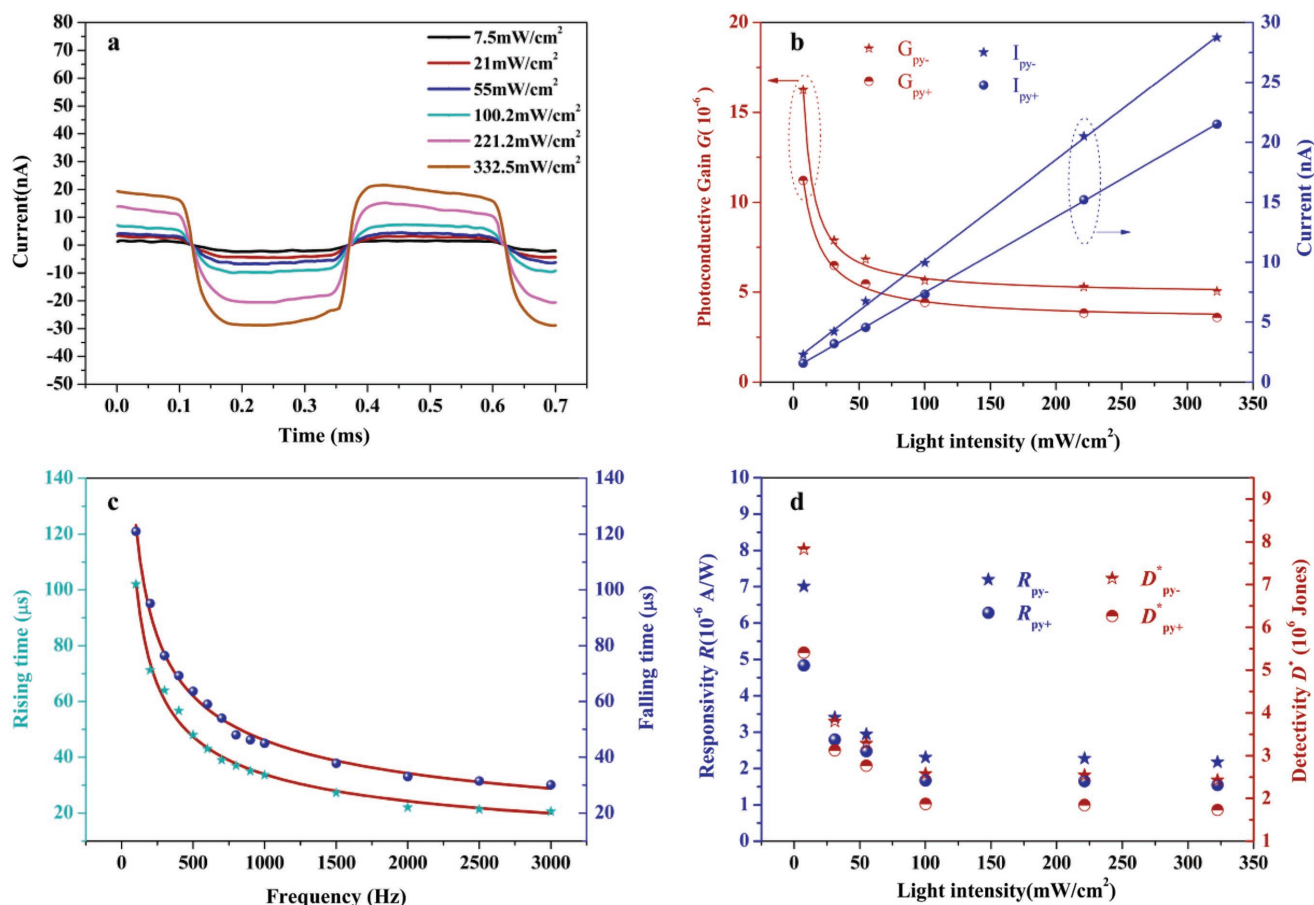


Figure 4. a) Current response of Au/CWQDs/Au photodetector under 532 nm illumination with different intensities from 7.5 to 322.5 mW cm⁻². b,c) Measured short-circuit current, photoconductive gain (G) and responsivity (R) of the positive and negative current under different light intensities of 532 nm illumination. c) The rising and falling time under different modulating frequency from 100 to 3000 Hz.

be 3.04×10^{-6} and 2.91×10^{-6} A W⁻¹, respectively. The experimental result has a certain extent of validation that the pyroelectric performance of the self-powered Au/CWQDs/Au PDs can be regulated by the modulation frequency.

In addition, the current response of the self-powered Au/CWQDs/Au PDs under continuous heating at 532 nm light modulated illumination by a 2 kHz frequency is measured and summarized in Figure S6 (Supporting Information), showing

that the transient current increases as the system temperature is increased from 22 to 34 °C. Figure 5b shows the current of the self-powered PDs at an instantaneous temperature. It is straightforward that the current I_{py} increases monotonically with the instantaneous temperature and they are approximately a strong linear relationship,^[36] the fitting line plotted in red, which shows the maximum of the pyroelectric current is 29.28 nA for I_{py-} and 25.18 nA for I_{py+} . Moreover, the enhancements of

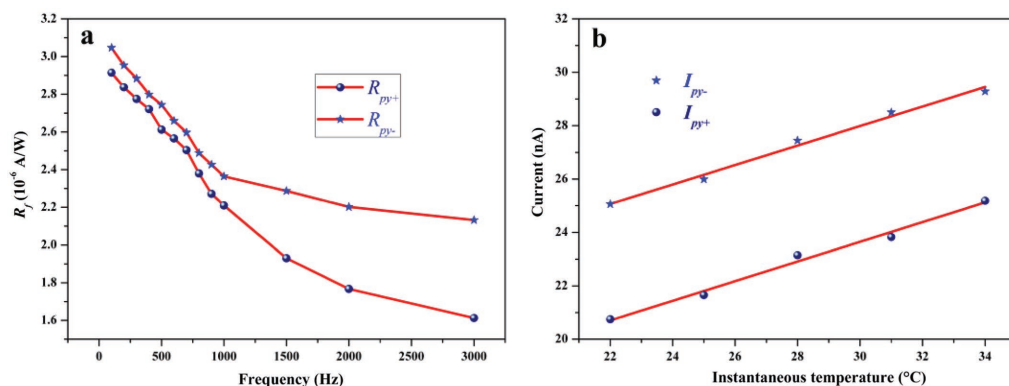


Figure 5. The positive and negative current under the modulation of a) frequency and b) temperature.

the current caused by heating are 19% for the I_{py-} and 21% for the I_{py+} , respectively. The PDs show a great potential application for temperature detection and energy harvest.

In conclusion, a novel low-cost, easy fabrication self-powered pyroelectric photodetector is demonstrated based on the colloidal wurtzite-structure CdSe/ZnS quantum dots and MEH-PPV. Under the modulated 532 nm light illumination, the device exhibits excellent photoinduced pyroelectric performance that the output current signal has rapid and sensitive response to the light intensity, frequency, and temperature. The edge-structure of PDs between the CWQDs and Au electrode provides long electrode spacing and low capacitance to obtain ultrafast response time with the rising time of 20.6 μ s and the falling time of 30.1 μ s. This work provides a brand new approach to achieve a self-powered 532 nm light photodetector based on photoinduced pyroelectric effect, which presents an extensive potential for the photodetectors, biological sensors, energy accumulators, and energy converters.

Experimental Section

Chemicals: All chemical reagents were of analytical grade and purchased from Aladdin, including acetone (98%), hexane (99.5%), toluene (98%), triethylphosphine (TOP, 90%), selenium (99.99%), 1-octadecene (ODE, 90%), stearic acid (SA, 99%), octadecylamine (ODA, 90%), triethylphosphine oxide (TOPO, 98%), cadmium oxide (CdO, 99.99%), sulfur (S, 99.99%), zinc oxide (ZnO, 99.99%), and oleic acid (99%).

Synthesis of CdSe QDs: The CdSe QDs were synthesized following the procedure reported before.^[37] First, the TOP-Se stock solution was prepared by mixing Se (0.158 g), TOP (1.421 g), and ODE (0.42 g) to obtain the transparent solution by the ultrasonic dissolving method. Then, CdO (0.2 mmol), SA (0.8 mmol), and ODE (2 g) were mixed in a three-necked round-bottom flask and the mixture was then heated to 200 °C until limpidity. Upon the mixture was cooled down to room temperature, ODA (1.5 g) and TOPO (0.5 g) were added into the mixture and heated to 280 °C. At the moment reaching the setting temperature, the prepared TOP-Se stock solution was injected rapidly and the reaction temperature was set to 250 °C for 2 min before turning off the heat and cooling to room temperature in the flask. The whole procedure was under argon. The prepared QDs solution was dissolved in n-hexane and then the toluene was injected to precipitating organic matter, repeated for three times. At last, a few acetone were added in the suspension which was centrifuged at 3000 rpm for 25 min. The remaining crimson precipitate decanted the supernatant was dissolved in hexane.

Synthesis of Wurtzite-Structure CdSe/ZnS QDs: ZnO (0.32 g), ODE (28 mL), and oleic acid (12 mL) were mixed in flask and heated to 300 °C under rapid stirring until dissolving to form a clear colorless Zn stock solution. The flask was then cooled to 200 °C and kept under argon until required. The mixture, including the synthesized CdSe QDs (2 mL), ODE (20 mL), and ODA (3 g), was slowly heated to 250 °C, followed by injection of the prepared Zn stock solution under continuous stirring for 10 min. After heating to 260 °C, 0.1 mol L⁻¹ S-ODE solution was injected and stirred for 20 min to form ZnS shell on QDs. The reaction was allowed to cool to room temperature and 20 mL of acetone was added to precipitate the extra ligand using centrifugation. The CdSe/ZnS QDs were kept in hexane for required.

Fabrication Process of the Au/CWQDs/Au PDs: The details of Au/CWQDs/Au photodetectors were fabricated as follows. The Au electrodes were thermally evaporated through a sophisticated shadow mask on the Si n⁺/SiO₂ substrate purchased from Six Carbon Technology Co., Ltd. Then, the CdSe/ZnS QDs were covered on the top by spin-coating at a speed of 3000 rpm min⁻¹. After 5 min of air drying, the film of MEH-PPV was deposited on the top of QDs film by the same spin-coating way. The

device was dried at 60 °C for 4 h and stored in vacuum conditions before further measurement.

Characterization and Testing: The absorption spectrum of CdSe/ZnS QDs and MEH-PPV was measured by a Zolix Omni- λ 3007 spectrophotometer. *I*-*V* characteristics of the PDs were tested by a Keithley 2400 with Labview software and the output current signal of the device was measured via a digital storage oscilloscope (Tektronix TDS 2022C) with an Ethernet connecting to a computer. The light source was sourced from a 532 nm semiconductor laser (ChangChun New Industries Optoelectronics Tech CO., LTD) and the light power was tested by a power meter with RS232 port (Ophir Vega). The periodic light illumination was used by a Model SR540 chopper controller (Stanford Research system, Inc.). The transmission electron microscope and atomic force microscope image of the device were obtained by an FEI Co., Tecnai G2 F20 TEM system at 200 kV and an atomic force microscope system (BY2000). The phase of QDs was characterized by the XRD (Cu K α radiation, λ = 1.5406 nm, D/MAX-2500-18 KW, Rigaku Corporation).

Supporting Information

Supporting Information is available from the Wiley Online Library or from the author.

Acknowledgements

This work was supported by the National Natural Science Foundation of China (Nos. 61675147, 61605141 and 61735010), Basic Research Program of Shenzhen (JCYJ20170412154447469), and Wenzhou City Governmental Public Industrial Technology Project (G20160014).

Conflict of Interest

The authors declare no conflict of interest.

Keywords

colloidal wurtzite-structure quantum dots, photodetectors, pyroelectric effect, self-powered devices

Received: May 15, 2018

Revised: July 22, 2018

Published online:

- [1] G. Vats, A. Kumar, N. Ortega, C. R. Bowen, R. S. Katiyar, *Energy Environ. Sci.* **2016**, *9*, 335.
- [2] S. Kim, Y. T. Lim, E. G. Soltesz, A. M. De Grand, J. Lee, A. Nakayama, J. A. Parker, T. Mihaljevic, R. G. Laurence, D. M. Dor, L. H. Cohn, M. G. Bawendi, J. V. Frangioni, *Nat. Biotechnol.* **2004**, *22*, 93.
- [3] S. Kundu, A. Patra, *Chem. Rev.* **2016**, *117*, 712.
- [4] G. B. Shen, C. Zhang, B. Zhang, M. Yuan, S. Yang, Y. Chen, *J. Appl. Phys.* **2014**, *115*, 19.
- [5] X. F. Wang, Y. J. Dai, R. Y. Liu, X. He, S. T. Li, Z. L. Wang, *ACS Nano* **2017**, *11*, 8339.
- [6] J. Briscoe, M. Stewart, M. Vopson, M. Cain, P. M. Weaver, S. Dunn, *Adv. Energy Mater.* **2012**, *2*, 1261.
- [7] S. K. Kim, C. V. Gopi, J. C. Lee, H. J. Kim, *J. Appl. Phys.* **2015**, *117*, 163104.

- [8] M. H. Sabina, B. Joe, S. Dunn, *Adv. Mater.* **2013**, *25*, 867.
- [9] Z. Y. Fan, D. W. Wang, P. C. Chang, W. Y. Tseng, J. G. Lu, *Appl. Phys. Lett.* **2004**, *85*, 5923.
- [10] A. Kumar, H. Gullapalli, K. Balakrishnan, A. B. Mendez, R. Vajtai, M. Terrones, P. M. Ajayan, *Small* **2011**, *7*, 2173.
- [11] T. Choi, S. Lee, Y. J. Choi, V. Kiryukhin, S. W. Cheong, *Science* **2009**, *324*, 63.
- [12] N. Ma, Y. Yang, *Nano Energy* **2017**, *40*, 352.
- [13] C. R. Bowen, J. Taylor, E. L. Boulbar, D. Zabek, V. Y. Topolov, *Mater. Lett.* **2015**, *138*, 243.
- [14] Y. Yang, J. H. Jung, B. K. Yun, F. Zhang, K. C. Pradel, W. Guo, Z. L. Wang, *Adv. Mater.* **2012**, *24*, 5357.
- [15] D. Zabek, J. Taylor, E. L. Boulbar, C. R. Bowen, *Adv. Energy Mater.* **2015**, *5*, 1401891.
- [16] S. Madan, J. Kumar, D. Madhwal, I. Singh, P. K. Bhatnagar, P. C. Mathur, *J. Nanophotonics* **2011**, *5*, 053518.
- [17] Y. Yang, W. Guo, K. C. Pradel, G. Zhu, Y. Zhou, Y. Zhang, Y. F. Hu, L. Lin, Z. L. Wang, *Nano Lett.* **2012**, *12*, 2833.
- [18] Y. Yang, S. Wang, Y. Zhang, Z. L. Wang, *Nano Lett.* **2012**, *12*, 6408.
- [19] G. Nasti, S. Coppola, F. Olivieri, V. Vespini, V. Pagliarulo, P. Ferraro, *Langmuir* **2018**, *34*, 2198.
- [20] S. H. Wang, A. Riedinger, H. B. Li, H. Y. Liu, L. L. Li, T. L. Liu, L. F. Tan, M. J. Batherl, G. Pugliese, F. De Donato, M. Scotto D'Abbusco, X. W. Meng, L. Manna, N. Meng, T. Pellegrino, *ACS Nano* **2015**, *9*, 1788.
- [21] S. S. Chou, B. Kaehr, J. Kim, B. M. Foley, M. De, P. E. Hopkins, J. Huang, C. J. Brinker, V. P. Dravid, *Angew. Chem.* **2013**, *125*, 4254.
- [22] J. D. Jackson, *Electrodynamics*, John Wiley & Sons, New York **1975**.
- [23] J. H. Lee, K. Y. Lee, M. K. Gupta, T. Y. Kim, D. Y. Lee, J. Oh, C. Ryu, W. J. Yoo, C. Y. Kang, S. J. Yoon, J. B. Yoo, S. W. Kim, *Adv. Mater.* **2014**, *26*, 765.
- [24] Z. L. Wang, *Mater. Today* **2017**, *20*, 74.
- [25] M. Sajid, M. Zubair, Y. H. Doh, K. H. Na, K. H. Choi, *J. Mater. Sci: Mater. Electron.* **2015**, *26*, 7192.
- [26] S. M. Hatch, J. Briscoe, S. Dunn, *Adv. Mater.* **2013**, *25*, 867.
- [27] X. Liu, L. L. Gu, Q. P. Zhang, J. Y. Wu, Y. Z. Long, Z. Y. Fan, *Nat. Commun.* **2014**, *5*, 4007.
- [28] M. P. Liu, J. H. Song, M. Y. Lu, M. T. Chen, Y. F. Gao, L. J. Chen, Z. L. Wang, *Nano Lett.* **2009**, *9*, 1223.
- [29] G. Cha, Y. S. Ju, *Sens. Actuators A* **2013**, *189*, 100.
- [30] K. Zhang, S. Wang, Y. Yang, *Adv. Energy Mater.* **2017**, *7*, 1601852.
- [31] X. Han, W. Du, R. Yu, C. Pan, Z. L. Wang, *Adv. Mater.* **2015**, *27*, 7963.
- [32] G. Konstantatos, E. H. Sargent, *Nat. Nanotechnol.* **2010**, *5*, 391.
- [33] Z. N. Wang, R. M. Yu, X. F. Wang, W. Z. Wu, Z. L. Wang, *Adv. Mater.* **2016**, *28*, 6880.
- [34] D. S. Zheng, H. H. Fang, P. Wang, W. J. Luo, F. Gong, J. C. Ho, X. S. Chen, W. Lu, L. Liao, J. L. Wang, W. D. Hu, *Adv. Funct. Mater.* **2016**, *26*, 7690.
- [35] C. G. Wu, W. L. Zhang, Y. R. Li, *Jpn. J. Appl. Phys.* **2006**, *43*, 2674.
- [36] N. T. Tien, Y. G. Seol, L. H. Anh Dao, H. Y. Noh, N. E. Lee, *Adv. Mater.* **2009**, *21*, 910.
- [37] Y. Chen, J. Vela, H. Htoon, J. L. Casson, D. J. Werder, D. A. Bussian, V. I. Klimov, J. A. Hollingsworth, *J. Am. Chem. Soc.* **2008**, *130*, 5026.

www.spm.com.cn